ELSEVIER

PII: S0032-3861(97)00409-6

Polymer Vol. 39 Nos. 6–7, pp. 1429–1437, 1998

0032-3861/97/$17.00+0.00

Crystallization thermodynamics and kinetics in semicrystalline diblock copolymers

I. W. Hamley[a], J. P. A. Fairclough[b], F. S. Bates[c] and A. J. Ryan[b,d,*]
[a]*School of Chemistry and Centre For Self-Organising Molecular Systems, University of Leeds, Leeds LS2 9JT, UK*
[b]*Manchester Materials Science Centre, UMIST, Grosvenor Street, Manchester M1 7HS, UK*
[c]*Department of Chemical Engineering and Materials Science, University of Minnesota, 421 Washington Avenue S.E., Minneapolis, MN 55455, USA*
[d]*CLRC Daresbury Laboratory, Warrington WA4 4AD, UK*
(Received 24 September 1996; revised 6 March 1997)

The crystallization of a series of diblock copolymers containing poly(ethylene) (PE) has been studied using simultaneous small-angle and wide-angle X-ray scattering (SAXS/WAXS). The PE crystalline domain thickness, obtained from a correlation function analysis of the SAXS data, was found for all samples to be independent of quench temperature because it is set by the branching density of the PE. In contrast to the PE crystalline domain thickness, the lamellar domain spacing of the homopolymers and block copolymers is found to decrease for deeper quenches, reflecting an increased degree of crystallinity of the PE. The equilibrium melting temperature of a PE homopolymer ($M_w = 23\,000$) prepared by hydrogenating poly(1,4-butadiene) is found to be significantly lower than that for linear PE due to chain folding induced by the short chain branches. The crystallization kinetics following quenches to different temperatures below the PE melting temperature have been analysed using the Avrami equation. For symmetric diblocks containing a rubbery amorphous block, a growth exponent $n = 3$ is found in the initial growth regime. A diblock containing glassy poly(vinylcyclohexane) (PVCH) amorphous blocks was also found to have $n = 3$, but the onset of crystallization was supressed to lower temperatures in the PVCH-containing sample, indicating that grafting the PE chains to glassy walls significantly retards the crystallization process. Comparisons of crystallization rates and growth mechanisms are made with high and low molecular weight PE homopolymers. The characteristic time for crystallization, extracted from the Avrami equation, was shown to follow Arrhenius behaviour as a function of temperature.

(Keywords: block copolymers; crystallization kinetics; morphology)

INTRODUCTION

Crystallization in block copolymers has attracted much interest recently because it enables preparation of nanoscale semicrystalline composites. We have shown in earlier work that microphase separation in the melt of a block copolymer is overwhelmed by poly(ethylene) (PE) crystallization below its melting point, T_m[1]. Structural changes in a range of diblock copolymers of poly(ethylene)-poly(ethylethylene) (PE-PEE) and poly(ethylene)–poly(ethylene-propylene) (PE-PEP) have been studied using simultaneous time-resolved small-angle X-ray scattering and wide-angle X-ray scattering. PEE and PEP were amorphous, having glass transition temperaures of $T_g = -20$ and -56°C, respectively. The degree of PE crystallinity in these diblocks was determined from differential scanning calorimetry (DSC) to be 40 ± 10%[1]. From SAXS, the lamellar structure formed by crystallization of a symmetric diblock copolymer was found to have a larger domain spacing than a melt lamellar phase, when the other component is amorphous. Asymmetric diblock copolymers containing an amorphous component that form hexagonal-packed cylinder (hex.) phases in the melt were also observed to form a lamellar phase with a different domain spacing on crystallization of the PE block. The solid structure could clearly be identified on the basis of multiple orders of Bragg reflections in the SAXS pattern as lamellae for a sample where PE was the minority component (volume fraction, $f_{PE} = 0.25$). In contrast, the presence of a single broad peak in the SAXS profile for an $f_{PE} = 0.75$ sample did not enable firm identification of the microstructure in this case, although it was clear that the high temperature melt hex. phase was destroyed[1].

Crystallization in diblock copolymers that form a homogeneous phase in the melt has also been studied[2,3] using SAXS/WAXS and DSC experiments on a range of poly(ethylene)–poly(ethylene-*alt*-propylene) diblock copolymers (PE-PE/P) with PE volume fractions ranging from $f_{PE} = 0.12$ to 0.56. For all the samples studied, crystallization occurred in a lamellar structure, and there was no indication of the formation of ordered structures in the melt[2]. In subsequent work[3], the dynamics of crystallization in several PE-PE/P and PE-PEE diblocks were studied and the development of up to four orders of SAXS peaks was found to be rapid and simultaneous following crystallization. During this process the location of the SAXS peaks was constant, suggesting a nucleation and growth process for the ordered structure. This is in agreement with our previous work, where the relative degree of crystallinity in PE-containing diblocks obtained from the WAXS data was shown to follow Avrami-type kinetics[1]. The exponent $n = 3.0 \pm 0.1$ found is consistent with a nucleation and growth process such as the formation of crystal spherulites.

* To whom correspondence should be addressed

Stem orientation in semi-crystalline diblock copolymers has been the subject of a number of investigations. Rangarajan *et al.* proposed a model in which the PE domain consists of crystallites with chains folded perpendicular to the interface alternating with amorphous regions[2]. However, oriented samples were not studied in that work. A similar orientation was found on the basis of SAXS/WAXS and electron microscopy data for solvent cast poly(ethylene oxide)-poly(isoprene) diblocks[4]. WAXS data was also consistent with perpendicular chain folding for low molecular weight poly(oxyethylene)-poly(oxybutylene) diblocks[5]. In contrast, Douzinas and Cohen reported parallel chain folding of poly(ethylene-*co*-butylene) (PEB) in PEB-PEE diblock copolymers on the basis of pole figure analysis of WAXS data[6]. This is in agreement with our recent results on diblocks shear oriented in ordered melt phases, where the stem orientation was unambigiously determined from the relative orientation of peaks in the two-dimensional SAXS/WAXS data obtained concurrently[7,8]. For symmetric diblocks containing PE and either an amorphous or a glassy block the PE stems were found to be parallel to the lamellar interface[8]. For a sample containing PVCH, which has a $T_g =$ 140°C, greater than T_m(PE), the constraint imposed by the glassy lamellar domains ensured that the poly(ethylene) crystallization did not change the domain spacing, but rather occured within the preexisting hard walls[7,8]. These hard walls also lead to lateral correlations between PE crystallites, as deduced from the presence of diffuse scattering bars parallel to the meridian for the PE-PVCH sample[7] that were not present for PE-PEE samples[8]. In the latter case the broad scattering peak in the SAXS pattern from semicrystalline PE was isotropic. For asymmetric diblocks forming a hex. phase in the melt, the solid structure was lamellae with the PE stems unoriented with respect to the lamellar interface[8]. However, in an $f_{PE} = 0.46$ sample forming a hexagonal perforated layer structure in the melt, chain folding parallel to the interface was observed, as for the symmetric samples forming lamellae in the melt[8].

We present results on the development of crystalline structure in PE-containing diblock copolymers following quenches below the PE crystallization temperature and the paper is organized as follows. SAXS profiles are presented for all sample and then analysed via the cosine-transform correlation. The development of the SAXS invariant, domain spacings and lamellar thickness during quenches to different temperatures below T_m(PE) are then discussed. Finally, we discuss the rates of crystallization of diblocks of different compositions and molecular weights, and the kinetics of crystallization in glassy *versus* amorphous environments is contrasted.

EXPERIMENTAL

Sample synthesis and characterization

Full details of the polymer synthesis and characterization are given elsewhere[9]. The number average molecular weights and compositions listed in *Table 1* were determined from the synthesis stoichiometry, which has been found to be a reliable measure of the molecular weight. Weight-average molecular weights for selected polyolefin diblocks or diene precursors were determined using light-scattering experiments. Molecular weight distributions were determined using size exclusion chromatography, and were found to be narrow ($M_w/M_n < 1.1$). The block microstructures were characterized using ^{1}H n.m.r., as described elsewhere[10]. The PE block in the PE-PEE diblocks is composed of a random distribution of poly(ethylene) and poly(ethylethylene) repeat units with 18 ethyl branches per 1000 backbone carbon atoms. The microstructure leads to a reduction in the melting temperature, degree of crystallinity and long period relative to high density (linear) poly (ethylene). For the PE homopolymer T_m is found to be typically 108°C (fully protonated version) with roughly 40% crystallinity. For the polyolefins containing PVCH a monodisperse poly(styrene)–poly(1,4-butadiene) diblock copolymer was anionically synthesized in cyclohexane using a lithium counterion. A two-step saturation process was completed using a homogeneous Wilkinson's catalyst, followed by a Pd/$BaSO_4$ heterogeneous catalyst to produce a poly(ethylene)-poly(vinyl cyclohexane) (PE-PVCH) diblock. A more detailed report discussing the two step saturation process has been given elsewhere[11]. This nearly symmetric sample is denoted PE-PVCH-1.

Table 1 Characteristics of the block copolymers

Sample	f_{PE}	M_n (kg mol^{-1})	Melt morphology	T_{ODT} (°C)
PE23k	1	23		
PE180k	1	180		
PE-PEE-2	0.55	20	Lamellae	$< T_{melt}$
PE-PEE-3	0.49	23	Lamellae	121
PE-PEE-22	0.50	81	Lamellae	> 300
PE-PEE-7	0.75	44	Hexagonal	148
PE-PVCH-1	0.52	15	Lamellae	238

f_{PE} = volume fraction of polyethylene in melt
M_n = number average molar mass by GPC
T_{ODT} = order disorder transition determined by rheology[10]

Synchrotron X-ray scattering

Simultaneous SAXS and WAXS experiments were performed on beamline 8.2 of the Synchrotron Radiation Source (SRS) at the Daresbury Laboratory, Warrington, UK. Details of the storage ring, radiation, camera geometry and data collection electronics have been given elsewhere[12]. The instrument is equipped with a multiwire quadrant detector for SAXS located 3.5 m from the sample position and a curved knife-edge WAXS detector that covers 120° of arc at a radius of 0.3 m. The samples for SAXS/WAXS were prepared by placing isotropic pieces of polymer cut from sheets into a cell comprising a Du Pont DSC pan fitted with windows ($\approx$ 6 mm diameter) made from 5 μm thick mica. Sealed pans were placed in a Linkam TMH600 hot-stage mounted on an optical bench. The design and operation of the X-ray DSC have been described in detail elsewhere[13]. A scattering pattern from an oriented specimen of wet collagen (rat-tail tendon) was used to calibrate the SAXS detector, while HDPE was used to calibrate the WAXS detector. A parallel plate ionization detector placed before the sample cell recorded the incident intensities. The experimental data were corrected for background scattering (from the camera, hot stage and empty cell), sample absorption and the positional alinearity of the detectors.

RESULTS

Representative SAXS profiles for PE homopolymer and PE-containing diblocks are presented in *Figure 1* as either the scattered intensity, I, or the Lorentz corrected scattered intensity, Iq^2 *versus* q (where $q = 4\pi\sin\theta/\lambda$ where 2θ is the scattering angle and λ is the X-ray wavelength). The SAXS

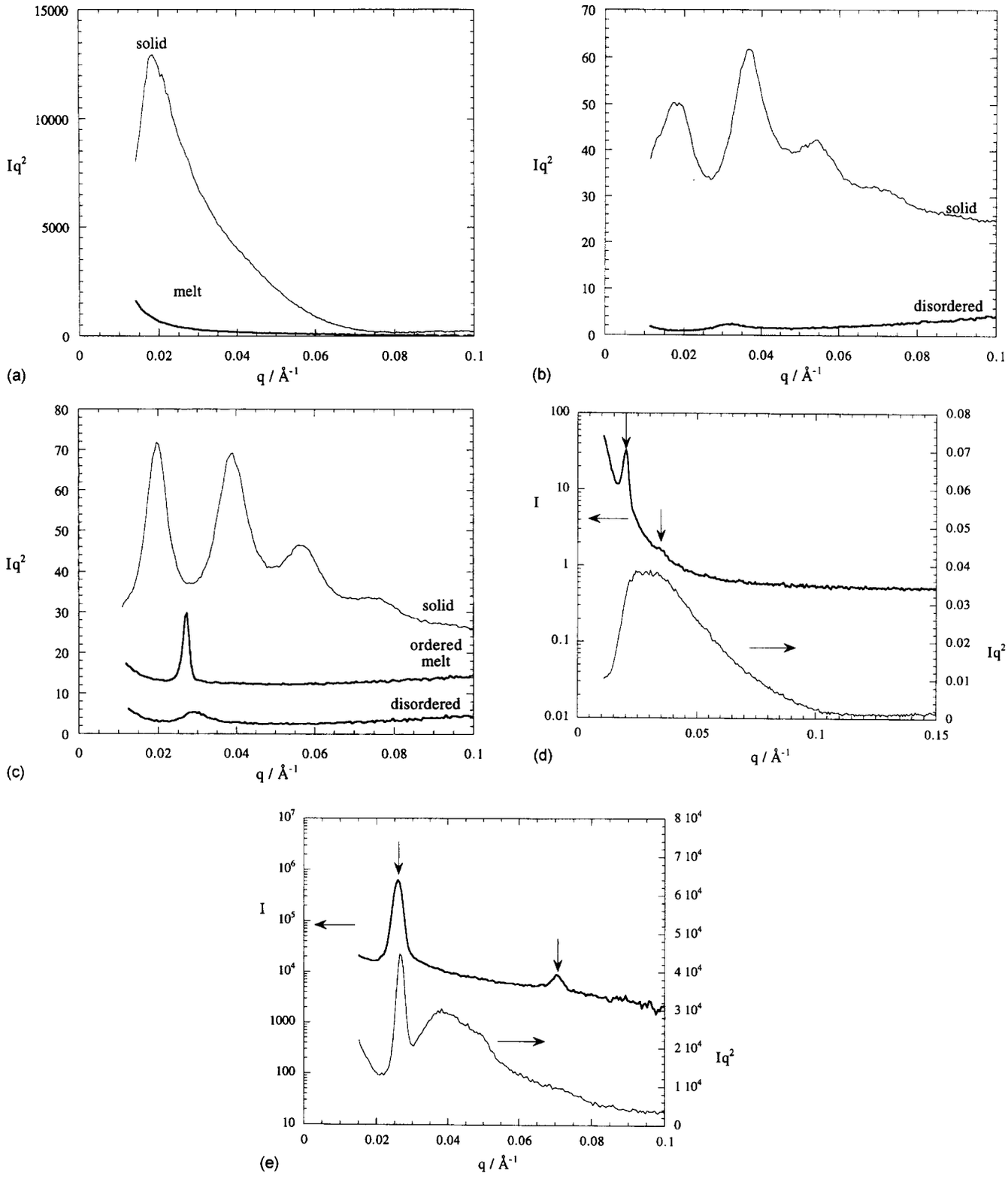

Figure 1 Lorentz-corrected SAXS intensity *versus* scattering vector magnitude for (a) PE23k (top profile at 104°C, bottom at 140°C); (b) PE-PEE-2 (both profiles at 95°C); (c) PE-PEE-3 (top two profiles at 100°C, bottom profile at 140°C); (d) PE-PEE-7 (top 140°C, bottom 100°C); (e) PE-PVCH (top 140°C, bottom 75°C). The intensities are in arbitrary units and the curves have been shifted for clarity

pattern for molten PE23k shown in *Figure 1*(a) is essentially featureless, simply displaying an increase at low q due to parasitic scattering (note that the data below $q = 0.013$ Å^{-1} is cut off by a beamstop). Upon crystallization, a broad, asymmetric peak characteristic of semicrystalline PE is formed. Similar scattering profiles were obtained for PE180k.

Small angle scattering data for two symmetric or nearly symmetric PE-PEE diblocks of increasing molecular weight are presented in *Figure 1*(b) and (c). The lowest molecular weight sample, PE-PEE-2, has an order–disorder transition, T_{ODT}, below T_m(PE). The SAXS pattern for the disordered melt contains correlation hole (or composition fluctuation) scattering[14] centred on $q = 0.032$ Å^{-1}. Upon crystallization,

several orders of Bragg reflection characteristic of a lamellar structure [*Figure 1*(b)] develop. The intensity of the second order reflection for PE-PEE-2 is higher than the first order, contrary to that observed for a melt lamellar structure, because scattering from semicrystalline PE leads to a broad peak centred on $q = 0.045$ Å^{-1}. PE-PEE-3 forms a lamellar phase below $T_{ODT} = 121$°C, and this is shown by a sharp Bragg reflection at $q^* = 0.027$ Å^{-1} in *Figure 1*(c). The SAXS data for the solid clearly indicates a lamellar structure, and the intensity of the second-order peak is distorted because of scattering from semicrystalline PE, as for PE-PEE-2. The location of the first order reflection, q^*, is at lower q than for the melt, and this shows the increase in domain spacing upon crystallization.

PE-PEE-22 has a molecular weight four times that of PE-PEE-2, and this results in a large increase in domain spacing upon crystallization. A broad scattering feature from semicrystalline PE in the lamellar solid[8] is observed in the SAXS data (not shown) similar to that obtained for the PE homopolymers. All the $f_{PE} \approx 0.5$ PE-PEE with rubbery amorphous blocks have a lamellar spacing in the solid which is larger than in the melt.

The asymmetric sample PE-PEE-7, with $f_{PE} = 0.75$, forms a hexagonal-packed cylinder phase in the melt[15]. The SAXS profile [*Figure 1*(d)] is consistent with this assignment, having peaks at q^* and $\sqrt{3}q^*$. The SAXS pattern changes upon crystallization to a broad asymmetric peak, which is dominated by semicrystalline PE scattering. We are unable to identify the morphology in the solid, although it is clearly not a highly ordered lamellar structure as formed by the symmetric samples. Additionally, in contrast to these samples, the domain spacing appears to decrease upon crystallization. This could reflect the degree of stretching of the chains prior to crystallization. This sample has a higher molecular weight than PE-PEE-2 and PE-PEE-3, and is therefore more strongly stretched at a given temperature in the melt than the low molecular weight polymers which have an approximately gaussian conformation. The gaussian chains are stretched by an amount proportional to temperature following a quench, as shown by the domain spacings, whereas the chain folding in the already stretched chains in PE-PEE-7 and PE-PEE-22 causes a reduction in domain spacing.

SAXS data for the symmetric diblock containing glassy PVCH are shown in *Figure 1*(e). This polymer forms a lamellar structure in the melt, as shown by SAXS on oriented samples [7,8]. First- and third-order reflections from this lamellar structure are indicated in *Figure 1*(e). The second-order reflection is absent due to a form factor minimum for this symmetric diblock. Crystallization occurs in this sample without change of domain spacing, as shown by the fixed location of the first order reflection, $q^* = 0.026$ Å^{-1} [*Figure 1*(e)]. The broad peak from semicrystalline PE that is centred on $q = 0.04$ Å^{-1} has a shoulder at high q that is likely to be a second-order reflection that develops on crystallization because f_{PE} then differs slightly from 0.5. These features in the SAXS profiles can be understood more quantitatively via an analysis of the cosine transform correlation functions, and we return to a discussion of these shortly.

A representative WAXS pattern (from PE-PEE7) is shown in *Figure 2*. Similar patterns were obtained for all polymers. In the melt, a broad peak is present which results from scattering from amorphous PE. Upon crystallization, (011) and (002) Bragg reflections are observed superimposed on the amorphous halo. These reflections are those

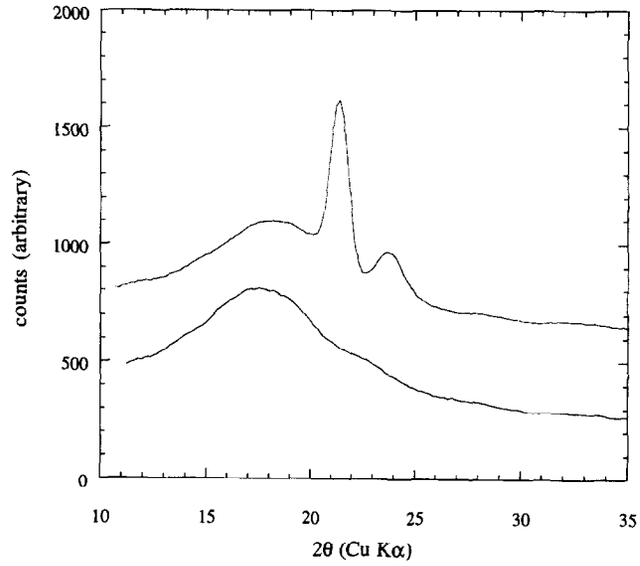

Figure 2 Representative WAXS patterns for PE-containing diblocks. Top, PE-PEE-7 at 100°C; bottom, PE-PEE-7 at 140°C.

observed for PE homopolymer and indicate that the PE crystallized in its usual orthorhombic form[16] for all samples.

The use of the one-dimensional correlation function is well established for the estimation of crystal thickness in semicrystalline polymers[17]. This method has been used[1] to estimate the crystal thickness in semicrystalline polymers using *a priori* knowledge of the crystal weight fraction from DSC. Scattering density correlation functions were computed from the SAXS data and the thickness of the crystalline PE region was determined from the extrapolated linear region of the density correlation function, $\gamma_1(r)$, using[17,18]

$$\gamma_1(r) = \frac{\int_0^\infty I(q)q^2\cos(qr)\,dq}{\int_0^\infty I(q)q^2\,dq} \quad (1)$$

The data was extrapolated to large q using a damped Porod function of the form

$$I(q) = \frac{K\exp(\sigma^2q^2)}{q^4} + I_b \quad (2)$$

where K is the Porod constant and I_b is a thermal density fluctuation background. Extrapolation to low q was performed using an intensity profile based on Guinier's law. Further details of this procedure are given elsewhere[18]. The extrapolated slope of the linear region of the correlation function before the first minimum is related to the size of the smallest scattering domain in the system[17], in this case the PE crystallizes[1].

Plots of the correlation function for PE and PE-PEE samples are shown in *Figure 3*. This immediately reveals qualitative differences between the structures of different samples. The shortest distance in the structure, l, is within the range 47 ± 5 Å for all homopolymer and copolymer samples, although PE23k and PE-PEE-22 are at the upper end of this range 51 ± 5 Å. This is the thickness of the PE domain because the PE degree of crystallinity, measured by DSC, $X_{PE} < 0.5$[1]. The location of the crystalline region within the PE domain cannot be deduced from a powder sample because any information on orientation is lost. The weak maximum in $\gamma_1(r)$ near 150 Å for the low molecular

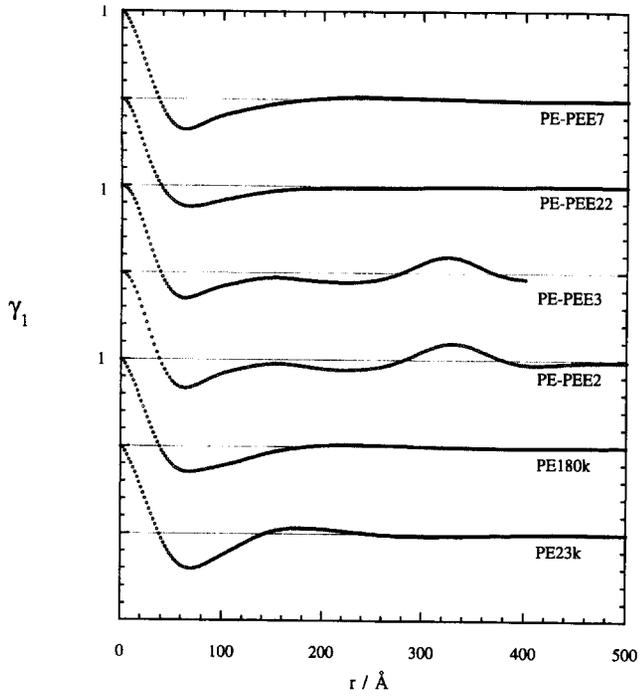

Figure 3 Cosine-transform correlation functions computed from the SAXS data for PE homopolymers and PE-PEE diblocks.

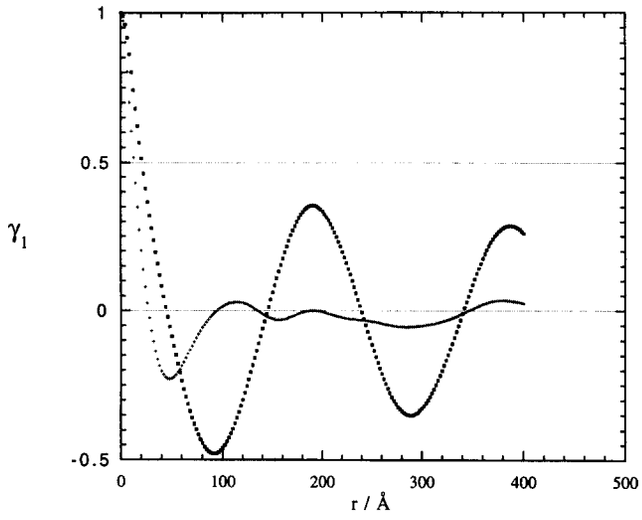

Figure 4 Cosine-transform correlation functions for PE-PVCH above T_m(PE) at 140°C (□) and in the solid at 75°C (×).

weight samples PE23k, PE-PEE-2 and PE-PEE-3 is due to the thickness d' of the amorphous + crystalline PE domain. For the samples which form lamellae, an additional peak in $\gamma_1(r)$ is observed with a position which matches closely that determined from $d = 2\pi/q^*$. This is the total lamellar period in the structure.

The correlation functions for PE180k, PE-PEE-22 and PE-PEE-7 (*Figure 3*) differ qualitatively from those for the lower molecular weight samples because the pronounced maxima at $r \neq 0$ are absent. This is a consequence of the SAXS profiles for these samples, which although they arise from distinct polymer architectures, namely a homopolymer, a symmetric diblock and an asymmetric diblock, respectively, all have a single asymmetric broad peak of scattering from semicrystalline PE. The lamellar structure is not sufficiently developed, as shown by the absence of higher-order Bragg reflections, to give a maximum in the correlation function corresponding to the domain spacing, d.

Cosine transform correlation functions for PE-PVCH are shown in *Figure 4*. When the PE is molten, the correlation function has a damped sinusoidal form, and this is consistent with a monodisperse lamellar structure with a sharp interface. Because the lamellar ordering is long range, the correlation function resembles a damped Patterson function for a layered system. This strongly segregated lamellar structure is likely to be caused by the hard glassy walls present at a temperature below T_g(PVCH). The correlation function for the crystallized sample is dramatically different. The first minimum corresponds to the PE crystal thickness and the first maximum to the thickness d' for the amorphous and crystalline PE domains. Subsequent maxima and minima are due to the long-range order imposed by the hard walls and coincide with $\gamma_1(r)$ from the copolymer with molten PE.

The small-angle scattering invariant (scattering power), lamellar spacing d and PE crystal thickness during heat/quench cycles are presented for representive polymers in *Figure 5*. The small-angle scattering invariant, Q, is a measure of the total small-angle scattering from a material, independent of the size or shape of structural inhomogencities[19]. It is then given by[20]

$$Q = \phi(1-\phi)\langle\eta^2\rangle = \frac{1}{2\pi i_e}\int_0^\infty I(q)q^2\,dq \qquad (3)$$

where ϕ is the volume fraction of a block, η is electron density difference between the blocks and i_e is the Thompson scattering factor. The absolute value of the invariant requires absolute intensity measurements. We have performed thermal background subtraction and extrapolation to $q = 0$ and $q = \infty$, but the data presented is in arbitrary intensity units.

In the case of symmetrical copolymers the crystallinity of the PE can be followed by the invariant. The $\phi(1-\phi)$ term is relatively insensitive to the small change in volume fraction on crystallization as $\phi \approx 0.5$. Formation of PE crystals causes the average electron density of the PE microphase to increase. In terms of density PVCH > xl-PE > am-PE > PEE, therefore crystallization causes η to increase in the PE-PEE polymers, but to decrease for PE-PVCH and the invariant is dominated by the square of the electron density difference η.

Using the length scales from the correlation function analysis, the local degree of crystallinity for the PE in the homopolymer can be estimated as $X = l/d$, whereas for the diblock it is approximately $X = l/(d\phi_{PE})$[21]. The invariant, domain spacing and PE crystallite thickness for PE23k are shown in *Figure 5*(a). The increase of the invariant following a quench below T_m(PE) follows Avrami-type kinetics, as discussed shortly. As expected, the invariant grows more rapidly for a deeper quench. Close to the measured melting point of PE (108°C) the invariant grows slowly, and the final degree of crystallinity is lower than for deeper quenches, as shown by the data at 106°C in *Figure 5*(a). The PE crystal thickness is seen to be essentially constant for the samples below T_m(PE), which is a consequence of the chemistry which introduces random ethyl branches in the PE. Conversely, the total domain thickness in the solid is proportional to the quench temperature. The dependence of domain spacing on annealing temperature can be used to estimate the equilibrium melting point of PE, and we return to this

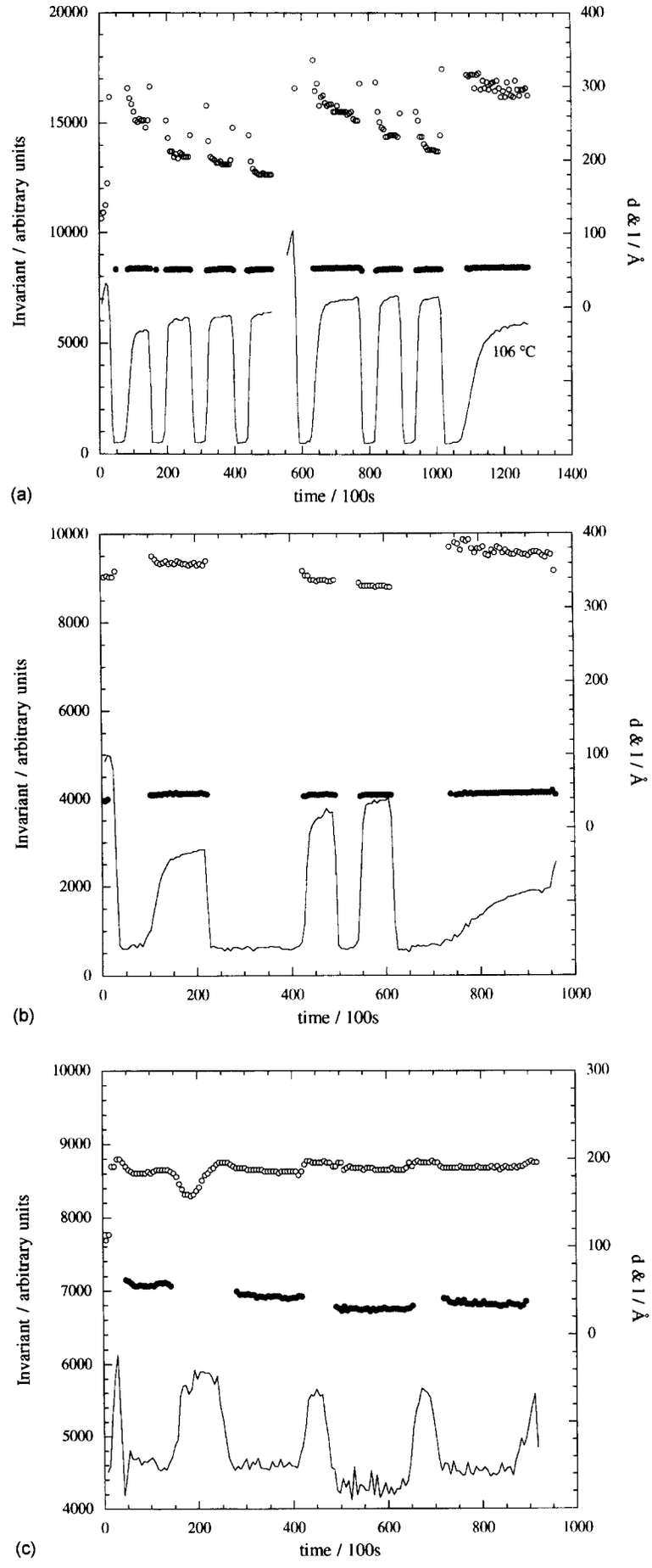

Figure 5 Small-angle scattering invariant (———), domain spacing (○) and PE lamellar thickness (●) *versus* time during a sequence of quenching experiments. The temperatures (in °C) following quenches from 140°C are indicated in parentheses. (a) PE23k (102, 96, 90, 85, 104, 100, 98, 106); (b) PE-PEE-2 (104, 100, 98, 106); (c) PE-PVCH (75, 60, 70, 65)

point shortly. Qualitatively similar trends of invariant and microstructure periods as a function of quench depth are observed for PE180k.

Representative data from the SAXS correlation function analysis for the diblock copolymers is presented for PE-PEE-2 in *Figure 5*(b) and PE-PVCH-1 in *Figure 5*(c). PE-PEE2, in *Figure 5*(b), shows similar trends to the data for the PE homopolymer. The relative degree of crystallinity $X = l/(d\phi_{PE})$, as mapped by the invariant, increases most rapidly, and to a higher value, for quenches to lower temperatures. The domain spacing of the solid is again proportional to the annealing temperature, whilst the PE crystallite thickness is independent of temperature, because it is largely controlled by the density of chain branches. The data for PE-PEE-22 (not shown) have similar trends to those already discussed, thus the highest temperature at which we were able to observed the onset of crystallization within the time-scale of the experiment for this sample (95°C) is lower than for the low molecular weight diblocks, and the rate of crystallization is dramatically slowed down at a given temperature. As discussed earlier in the context of the correlation functions, the domain spacing is not well defined upon crystallization of this polymer. The data for the asymmetric diblock PE-PEE-7 (not shown) also have similar trends to those for the low molecular weight symmetric samples. In each case fits to plots of the relative degree of crystallinity as a function of time following a quench using the Avrami equation yield exponents of $n \approx 3$, as discussed shortly.

The sample PE-PVCH-1 was initially heated into the isotropic phase 280°C prior to the series of annealing experiments shown in *Figure 5*(c) to destroy previous orientation of the lamellar phase in this sample[1]. The data in *Figure 5*(c) reveal that this sample behaves very differently below T_g(PVCH) compared to those containing a rubbery block. As noted earlier, the total domain thickness does not change upon crystallization due to the constraint imposed by the hard glassy walls. The PE lamellar thickness, $l \approx 35$ Å, appears to be smaller than for the block copolymers with rubbery amorphous blocks and shows greater temperature sensitivity, which is an effect of the constraint provided by the glassy walls. The most dramatic feature of this data, however, is that the temperature required for crystallization to occur, and the rates of crystallization are much lower than for the PE-PEE samples. This presumably reflects the lowering of the PE crystallization temperature in the nanoscale-confined space between glassy PVCH domains. This may be due to the increase in excluded volume of the polymer chains imposed by the confinement.

The equilibrium melting temperature, T_m^0 of the branched PE can be estimated from a plot of quench temperature as a function of domain spacing. As shown in *Figure 6*, there is a linear relationship between the inverse domain spacing and annealing temperature for PE23k. A linear relationship between inverse crystal thickness and melting temperature is predicted by the Thompson–Gibbs equation for crystalline polymers[22]. Analysis of the slope in terms of the theoretical parameters is complicated in our case, because we are not measuring crystal thickness and melting temperatures, but rather long spacing and crystallization temperature. Nonetheless, extrapolation of the line yields an estimate of $T_m^0 = 128$°C. This compares to the literature value for PE, $T_m^0 = 141$°C[23]. The difference is because the present PE is not linear, and therefore cannot achieve long-fold lengths as folding is not kinetically controlled, but dominated by the ethyl chain branches introduced in the synthesis procedure.

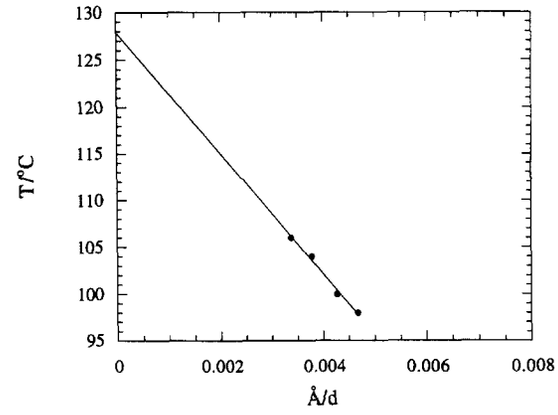

Figure 6 Annealing temperature *versus* the reciprocal domain spacing for PE23k. Extrapolation to infinite thickness gives T_m^0.

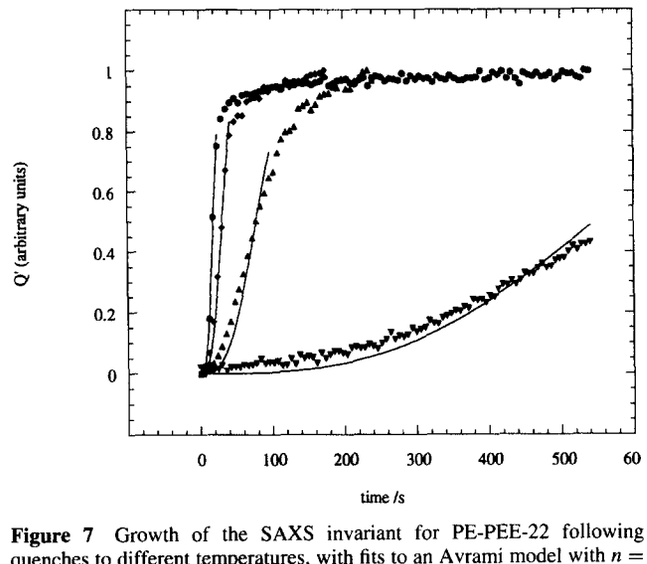

Figure 7 Growth of the SAXS invariant for PE-PEE-22 following quenches to different temperatures, with fits to an Avrami model with $n = 3$: (●) 75°C; (■) 80°C; (▲) 90°C; (▼) 95°C.

The change in the SAXS invariant during crystallization is proportional to the relative degree of crystallinity [see equation (3)], and was fitted for all samples using an Avrami equation for the PE and PE-PEE polymers,

$$Q'v = 1 - \exp(-kt^n) \tag{4a}$$

and a modified equation for the PE-PVCH,

$$Q' = \exp(-kt^n) \tag{4b}$$

where Q' is the SAXS invariant normalized to $Q' = 1$ at long times, k is a rate constant and the exponent n is a function of the nucleation and growth mechanism (dimensionality and whether thermal or athermal). For all polymers, we determined k by fixing $n = 3$ in the initial crystallization regime. This is the exponent we found previously for PE-containing diblock copolymers, and is consistent with spontaneously nucleated sphereulitic growth. However, this exponent does not describe the secondary growth of crystallites, and for this reason we have only fitted the data for the initial crystallization process. Good fits were obtained for all polymers, including the sample with glassy walls PE-PVCH-1, and we return to a discussion of this samples shortly. A representative fit, for PE-PEE-22, is shown in *Figure 7*, and this may be compared to the fits for the PE180k homopolymer shown in *Figure 8*. The

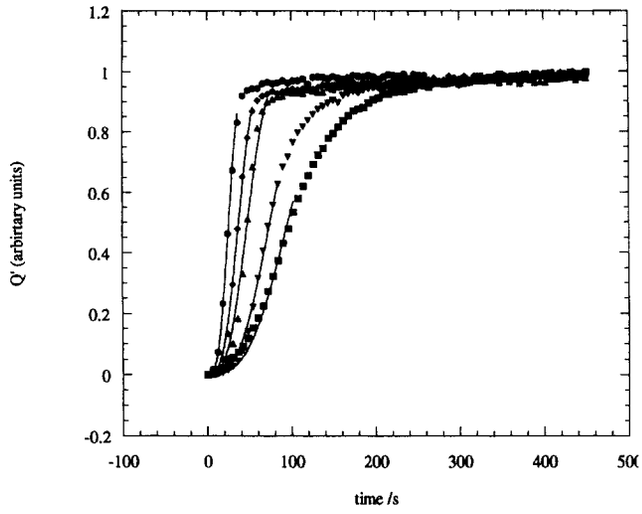

Figure 8 Growth of the SAXS invariant for PE180k following quenches to different temperatures, with fits to an Avrami model with $n = 3$: (●) 86°C; (◆) 88°C; (▲) 90°C; (▼) 92°C; (■) 95°C.

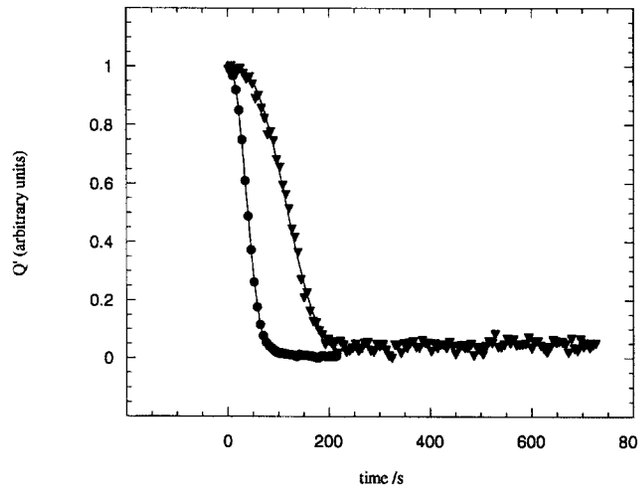

Figure 9 Reduction of the normalized invariant as a function of time for PE-PVCH1, following quenches to (●) 50°C and (▼) 92°C.

crystallization data for PE-PVCH-1 is shown in *Figure 9*. The invariant falls during the crystallization process as the electron density difference of the PVCH and PE microphases is reduced. The Avrami equation actually gives a much better fit to these data sets than those from polymers which do not have confining glassy walls and we speculate that there is a different crystallization mechanism here of heterogeneously nucleated two-dimensional growth.

The characteristic times $\tau = 1/k$ extracted from the Avrami fits with n fixed equal to 3 were determined as a function of temperature. *Figure 10* illustrates that Arrhenius behaviour is exhibited for all samples. With the exception of the data for PE-PVCH-1, the slopes of the straight lines obtained from an Arrhenius equation

$$\tau = A\exp(-E_a/RT), \quad (5)$$

where A is a pre-exponential factor, plotted on a semi-logarithmic graph are approximately the same, and yield values for E_a in the range 2.5 ± 0.7 kJ mol^{-1}. For PE-PVCH, the activation energy is much lower, $E_a \approx 0$ kJ mol^{-1}, although crystallization only occurs at much lower temperatures than for the other samples. Interpretation of these activation

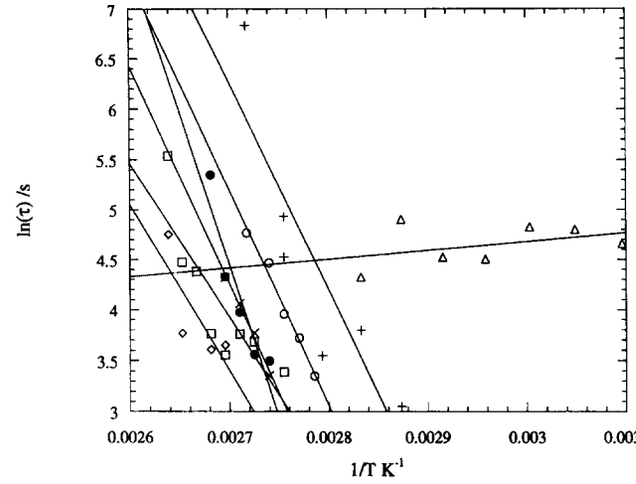

Figure 10 Arrhenius plots of the characteristic crystallisation time (τ) *versus* reciprocal quench depth for (□) PE23k, (○) PE180k, (◇) PE-PEE-2, (×) PE-PEE-7, (+) PE-PEE-22, (Δ) PE-PVCH-1, (●) PE-PEE-3

energies is complicated because the overall crystallization rate in polymers is a function of segmental flexibility, the rate of short-range transport of the crystallizing segments and of the nucleation rate (a general expression is given by Gedde[22]). However, we note that the experimental activation energies are comparable to the heat of fusion of crystalline polymers, and may be compared with a value $\Delta H = 4.11$ kJ mol^{-1} for the PE homopolymer[22].

PE-PVCH-1 differs from the other samples because it contains a glassy component and the crystallization temperature and kinetics were found to be quite different to the other samples. For example, a much greater undercooling was required to crystallize the PE-PVCH-1 material and the crystallization kinetics were far less temperature sensitive. It is surmised that the presence of a glassy component inhibits nucleation and growth of spherulites, but instead leads to solid sheafs.

SUMMARY

We have shown that the PE domain thickness is independent of crystallization quench depth for a range of diblock copolymers and homopolymers. In contrast the lamellar domain spacing is a sensitive function of crystallization temperature because it depends on the degree of crystallinity that increases for deeper quenches.

The crystallization kinetics of symmetric diblock copolymers containing rubbery and glassy amorphous components are well represented by Avrami equations with $n = 3$ in the primary growth regime. For the diblock copolymers containing rubbery amorphous components this was interpreted as random nucleation and growth in spherulites in light of previous microscopy results. For a sample containing glassy PVCH, nucleation and growth of spherulites is suppressed by the presence of the glassy lamellae, but still leading to exponents $n = 3$. Crystallization in this sample was also observed only for much deeper quenches than for the other polymers studied here, suggesting that its onset is hindered by the presence of glassy walls (formed by PVCH lamellae). Electron microscopy experiments are presently in progress to confirm these observations. Arrhenius plots of the characteristic crystallization time as a function of inverse temperature for all symmetric diblocks and PE homopolymers give an estimate

of the activation energy for crystallization of 2.5 ± 0.7 kJ mol^{-1}. In the case of PE-PVCH-1, the characteristic crystallization time is independent of temperature within experimental error. This temperature insensitivity is caused by the pinning of the PE block by the joint at the interface restricting the mobility of the entire block.

ACKNOWLEDGEMENTS

IWH, JPAF and AJR thank the EPSRC (UK) for support (grant GR/K05982). We are grateful to Dr B.U. Komanschek (Daresbury Laboratory) for help with the X-ray experiments and the Materials SESS for the allocation of beamtime.

REFERENCES

1. Ryan, A. J., Hamley, I. W., Bras, W. and Bates, F. S., *Macromolecules*, 1995, **28**, 3860.
2. Rangarajan, R., Register, R. A. and Fetters, L. J., *Macromolecules*, 1993, **26**, 4640.
3. Rangarajan, R., Register, R. A., Adamson, D. H., Fetters, L. J., Bras, W., Naylor, S. and Ryan, A. J., *Macromolecules*, 1995, **28**, 1422.
4. Hirata, E., Ijitsu, T., Soen, T., Hashimoto, T. and Kawai, H., *Polymer*, 1975, **16**, 249.
5. Yang, Y.-W., Tanodekaew, S., Mai, S.-M., Booth, C., Ryan, A. J., Bras, W. and Viras, K., *Macromolecule*, 1995, **26**, 6029.
6. Douzinas, K. C. and Cohen, R. E., *Macromolecules*, 1992, **25**, 5030.
7. Hamley, I. W., Fairclough, J. P. A., Ryan, A. J., Bates, F. S. and Towns-Andrews, E., *Polymer*, 1996, **37**, 4425.
8. Hamley, I. W., Fairclough, J. P. A., Terrill, N. J., Ryan, A. J., Lipic, P., Bates, F. S. and Towns-Andrews, E., *Macromolecules*, 1996, **27**, 8835.
9. Rosedale, J. H., Bates, F. S., Almdal, K., Mortensen, K. and Wignall, G. D., *Macromolecules*, 1995, **28**, 1429.
11. Gehlsen, M. D. and Bates, F. S., *Macromolecules*, 1993, **26**, 4122.
10. Bates, F. S., Rosedale, J. H., Bair, H. E. and Russell, T. P., *Macromolecules*, 1989, **22**, 2557.
12. Bras, W., Derbyshire, G. E., Ryan, A. J., Mant, G. R., Felton, R. A., Lewis, R. A., Hall, C. J. and Greaves, G. N., *NIMPR*, 1993, **A326**, 587.
13. Bras, W., Derbyshire, G. E., Cedie, J., Komanschek, B. E., Devine, A., Clark, S. M. and Ryan, A. J., *Journal of Applied Crystallography*, 1995, **28**, 26.
14. Leibler, L., *Macromolecules*, 1980, **16**, 1302.
15. Hamley, I. W., Gehlsen, M. D., Khandpur, A. K., Koppi, K. A., Rosedale, J. H., Schulz, M. F., Bates, F. S., Almdal, K. and Mortensen, K., *Journal of Physics (France) II*, 1994, **4**, 2161.
16. Brandrup, J. and Immergut, E. H., ed., *Polymer Handbook*, 3rd edn. Wiley, New York, 1989.
17. Strobl, G. R. and Schneider, M., *Journal of Polymer Science*, 1980, **18**, 1343.
18. Ryan, A. J., Stanford, J. L., Bras, W. and Nye, T. M. W., *Polymer*, 1997, **38**, 759.
19. Balta-Calleja, F. J. and Vonk, C. G., *X-ray Scattering of Synthetic Polymers*. Elsevier, New York, 1989.
20. Ryan, A. J., Naylor, S., Komanschek, B., Bras, W., Mant, G. R. and Derbyshire, G. E., *ACS Symposium Series*, 1994, **581**, 162.
21. Wutz, C., Bark, M., Cronauer, J., Döhnnann, R. and Zachmann, H. G., *Review of Science Instruments*, 1995, **66**, 1303.
22. Gedde, U. W., *Polymer Physics*. Chapman and Hall, London, 1995.
23. Wunderlich, B., *Macromolecular Physics: 3. Crystal Melting*. Academic, New York, 1980.